ACS APPLIED MATERIALS & INTERFACES

Research Article

www.acsami.org

Homogeneous Surface Oxidation of Organosilicates by Controlled Combustion of Adsorbed Fuels: A Facile Method for Low-Temperature Processing

Bob E. Feller,[†] Vaughn R. Deline,[†] John Bass,[†] André Knoesen,[‡] and Robert D. Miller*,[†]

[†]IBM Almaden Research Center, 650 Harry Road, San Jose, California 95120, United States

[‡]Department of Electrical and Computer Engineering, University of California, Davis, California 95616, United States

Supporting Information

ABSTRACT: We have developed a method for the oxidation of organosilicate materials at temperatures considerably lower than those typically required for uncatalyzed oxidation. The process utilizes a combustible fuel delivered to the surface in an oxidizing environment to locally oxidize materials with carbon−silicon bonds. It also provides a level of control that cannot be achieved through standard high-energy top-to-bottom oxidative procedures such as UV−ozone and O_2 plasmas. While the latter processes attack the outer interface, local oxidation can be achieved using our process by manipulating the distribution of the combustible fuel. We use this technique to generate oxidized porous organosilicate films with either a sharp oxidation front or uniform oxidation where the relative carbon content can be controlled through the film thickness depending on processing conditions. Further, we show that this process can also be used to seal bulk interconnected microporosity in films (<1 nm) without substantially changing the refractive index of the material. For both the nominally dense and porous films, the surface oxidation is accompanied by an increase in the Young's modulus and the oxidized films can be readily functionalized using standard silane chemistry to provide a variety of chemical functionalities.

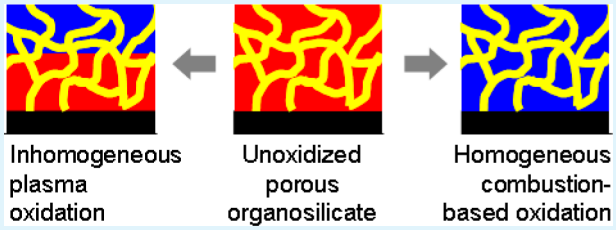

KEYWORDS: *organosilicate, oxidation, controlled combustion, homogeneous oxidation, porous, SIMS*

INTRODUCTION

Silsesquioxanes (SSQs) make up an important class of silicon-containing materials used in a wide range of applications in microelectronics,[1] photonics,[2,3] the biomedical field,[4,5] and catalysis.[5] Spin-on-dielectrics based on silsesquioxanes have most frequently been employed previously for gap filling and planarization.[6,7] With the addition of a sacrificial pore generator (porogen), these silsesquioxanes can be made porous to reduce their dielectric constant for low-k applications.[8,9] Further, hydrogen silsesquioxane is a common resist material of exceptional sensitivity used in e-beam lithography.[10] Because of the considerable number of applications of silsesquioxane materials, processes that can modify these materials in a controllable and reproducible fashion are valuable.

Recently, numerous reports of porous silica-based thin films prepared by a sol−gel process have been used to enhance the detection of low-molecular weight proteins in serum.[11−13] Porous thin films prepared in this manner from tetraalkoxysilanes by hydrolysis yield hydrophilic films and therefore are easily wet by aqueous media. This characteristic is necessary for aqueous biosensing applications. However, these silica sol−gel films have been shown to be unstable under physiologically relevant conditions (mildly alkaline) because of the acidity of the silanol functionality and therefore are not be suitable for extended studies in biological media.[14,15] Another drawback of the silica sol−gel materials and process is that these casting solutions are chemically unstable to aggregation and gelation and need to be used shortly after mixing.

In contrast, silsesquioxane solutions can be stable for months under suitable conditions, making them attractive starting materials for the preparation of cross-linked organosilicate resins. Further, the incorporation of carbon-containing substituents increases the hydrophobicity and imparts hydrolytic stability to the respective coatings.[16] However, these materials are typically very hydrophobic after curing, and hydrophobic porous films do not readily fill with water.[17] While this is advantageous for low-k applications, it is not useful for biosensing.

Methods such as UV−ozone and O_2 plasma treatment are typically employed for oxidizing silsesquioxane-based materials to provide functionality and improve adhesion.[18−20] These methods are particularly aggressive, producing both radicals and ions in the gas phase that cause extensive damage to the organosilicate film upon impact and are difficult to control.[21] Because the reactive oxidizing species in these processes are generated in the gas phase, damage is more likely to occur first at the gas−solid interface, creating materials with nonuniform properties through the thickness of the film with overoxidation at the interface.[22,23]

Received: June 19, 2013
Accepted: August 29, 2013
Published: September 16, 2013

   dx.doi.org/10.1021/am4023237 | *ACS Appl. Mater. Interfaces* 2013, 5, 9075−9087

Here we describe a thermal method for oxidizing cured organosilicate films at relatively low temperatures that provides control over both the extent and uniformity of oxidation. The procedure for uniform oxidation is most useful for the transformation of porous samples. The technique uses a combustible fuel and an oxidizer to locally oxidize the organosilicate surface. Depending on the conditions, the transformation can proceed like the UV−ozone and O_2 plasma processes in which oxidation occurs initially at the outer interface, creating a sharp oxidation front even in porous samples. Alternatively, the fuel source can be uniformly distributed throughout the porous material prior to combustion, leading to a uniform oxidation profile across the thickness of the film. Here, the spatial oxidation is governed by the regional presence of the fuel. This treatment is particularly efficacious for the uniform transformation of high-surface area porous materials. We believe this level of control and versatility will be useful in numerous applications, including microelectronics, photonics, biomedicine, etc., where controlled surface functionalization is critical.

EXPERIMENTAL SECTION

Materials. Octane, propylene glycol monomethyl ether acetate (PGMEA), and cyclohexanone were used as received from Sigma-Aldrich. Toluene was also received from Sigma-Aldrich and distilled prior to use. Poly(styrene-*b*-4-vinyl pyridine) was purchased from Polymer Sources, and Pluronic L121 was purchased from BASF.

Organosilicate Film Formation. The organosilicate used in these studies was generated from a methylsilsesquioxane PMSSQ copolymer with a molecular weight of approximately 2K generated from a methyltrialkoxysilane/tetraalkoxysilane mixture at a molar ratio of 3:1. The PMSSQ stock solution provided by JSR Corp. was ∼20 wt % solids in propylene glycol propyl ether. A poly(styrene-*b*-4-vinyl pyridine) with a styrene-block molecular weight of 19K and a 4-vinyl pyridine-block molecular weight of 5K from Polymer Sources and Pluronic L121 from BASF composed of ethylene glycol and propylene glycol blocks with an overall average molecular weight of 4.4K were used as porogens. Films were prepared by spin-casting at 2000 rpm for 60 s from solutions prepared with 10 wt % solids of either PMSSQ or PMSSQ/polymer mixtures. The 10 wt % spinning solution was prepared as follows for each film and was typically prepared on a 5−10 mL scale. The spinning solution for the nominally dense organosilicate film (microporous upon curing) was prepared by diluting the stock solution of PMSSQ to 10 wt % with propylene glycol monomethyl ether acetate (PGMEA). For the sake of convenience, these films are denoted as MSSQ. Two different porous films were used in this study. The spinning solution for the first porous film was prepared by mixing a solution of the MSSQ and the polymer. The stock PMSSQ was diluted to 10 wt % with cyclohexanone, and poly(styrene-*b*-4-vinyl pyridine) was dissolved in cyclohexanone at 10 wt %. These were then mixed at a 2:3 polymer:MSSQ ratio to obtain a solution in which the solid is 40% poly(styrene-*b*-4-vinyl pyridine). These films prepared by spin-casting from this solution are designated as PS-P4VP/Si. The other porous film was prepared by diluting the stock PMSSQ to 10 wt % with PGMEA and preparing a 10 wt % solution of Pluronic L121 in PGMEA. These were mixed to the same solid concentration of the polymer. The spin-cast films are designated L121/Si. All films were initially baked at 450 °C for 2 h in a nitrogen environment after a ramp rate of 5 °C/min to the maximal temperature to set the organosilicate and decompose the porogen.

Experimental Setup. Silsesquioxane curing, porogen decomposition, and organosilicate oxidation were performed on a Cimarec 2 hot plate. An aluminum block with an embedded thermocouple was placed on the hot plate, and the temperature was controlled using an Omega temperature controller. The samples were placed directly on the aluminum block and covered with a Pyrex crystallizing dish with a ground glass joint on the top of the cover through which vapors make contact with the samples. For silsesquioxane curing and porogen decomposition, the samples were heated under nitrogen to 450 °C for 2 h at a rate of 5 °C/min before cooling to room temperature. For the organosilicate oxidation studies, all samples were previously cured in pure nitrogen. Oxidation samples were heated to 450 °C and maintained at this temperature; alternatively, the temperature was cycled between two temperatures with a high−low difference of ∼50 °C. For the constant-temperature experiments, the conditions were identical to those of the silsesquioxane curing step except that the vapor can be either nitrogen or pure oxygen and a hydrocarbon fuel (nominally octane) may be present. To introduce hydrocarbon fuels at varying fractions of room-temperature saturation levels, two mass flow controllers were used where the outlet of one was passed through a bubbler with the liquid fuel (e.g., octane). The stream leaving the bubbler was assumed to be 100% saturated at room temperature (abbreviated $P_{sat}|^{25C}$) and mixed with the stream containing no hydrocarbon. The mass flow controllers were adjusted to vary the concentration relative to saturation ($P_{concl}|^{25C}$). For the temperature cycling experiments (*vide infra*), one carrier gas stream was passed through the bubbler and assumed to reach $P_{sat}|^{25C}$. The temperature was rapidly increased to an initial temperature 50 °C below the maximal temperature of the experiment, further increased to the maximal temperature over a 10 min period, and then decreased to the initial temperature (50 °C below the maximum) over 15 min. This constitutes one temperature cycle, and for each experiment, the cycle was repeated eight times before the samples were cooled to room temperature. For example, if the maximal temperature was 280 °C, the temperature was increased from 230 to 280 °C over 10 min and returned to 230 °C over 15 min. In the analysis of oxidation trends, measurements (contact angle, thickness, refractive index, and pore size) represent a single sample for each experimental condition. To ensure that films were identical initially, each series was cast from the same solution batch. In our experience, multiple measurements within a single sample and between different samples were extremely consistent (<10% variation).

Ellipsometric Porosimetry. Ellipsometric porosimetry measurements were conducted using toluene on a home-built apparatus based on the design of Baklanov et al.[24] utilizing a commercial spectroscopic ellipsometer (Woollam M-2000V and WVASE32 acquisition software). The sample chamber was constructed of anodized aluminum with windows perpendicular to the beam at a fixed angle of 75°. Vacuum was applied using a Welch Duoseal 1376 pump. The toluene partial pressure was regulated using two MKS 248A control valves located before and after the sample chamber to control the inlet and outlet flow rates, respectively. A manometer measured the chamber pressure, and software (Labview) controlled the two valves to achieve the desired pressure.

It should be noted that the refractive indices of all films were calculated using a one-layer model. SIMS analysis of the element composition indicated that three samples (MSSQ in O_2 with octane at $P_{0.025\%}|^{25C}$ and PS-P4VP/Si in O_2 with octane at $P_{0.025\%}|^{25C}$ and $P_{0.25\%}|^{25C}$) displayed layered behavior (*vide infra*). However, because of the similarities in the refractive index of these two layers, we were unable to obtain consistent fits with a two-layer model, and therefore, a one-layer model provided an accurate approximation. Similarly, modulus values were analyzed in the same manner. Toluene-filled pores of the nitrogen-cured and oxidized samples have nearly identical refractive indices, making the layers indistinguishable when assessed by ellipsometry. Thus, the one-layer model will provide an accurate measurement of film thickness and, therefore, modulus.

Secondary Ion Mass Spectroscopy (SIMS). The secondary ion mass spectrometry (SIMS) measurements were obtained with the use of a Cameca SC-Ultra instrument. The bombarding ion was Cs^+ at 2 keV with a current of approximately 30 nA. The beam raster was 500 μm square, and secondary ions (CsC^+, CsO^+, and $CsSi^+$) were detected from a 50 μm diameter at the center of the raster. The extent of surface charging was reduced with the use of an electron beam at 3 keV. Quantification of the C, O, and Si signals was accomplished by determining the secondary ion yield ratios from reference MSSQ films (450 °C in N_2 and 450 °C in O_2 with $P_{25\%}|^{25C}$) and assuming the ratios were constant over the range of compositions. The ratios were not constant as the signals progressed into the Si substrate, resulting in inaccuracies in the Si substrate concentration.

RESULTS AND DISCUSSION

This oxidation process was initially discovered serendipitously during a study of the surface energy of porous films cured at 450 °C for 2 h. Films cured in a high-purity nitrogen environment had a low surface energy (high water contact angle), as expected. However, films cured in laboratory air had a much higher surface energy, and water would either partially or completely wet the surface. Thinking oxygen was the cause, we designed a system to control the relative oxygen concentration using a clean oxygen source. Curiously, under these conditions, even films that were cured in pure oxygen still had a low surface energy. Finally, it was determined that combustible, organic contaminants in the laboratory air, in the presence of oxygen, were responsible for the increase in surface energy. The following describes a series of experiments designed to exploit this process using octane and oxygen as the fuel and oxidizer, respectively.

Experimentally, the process of low-temperature organosilicate oxidation is very straightforward. The oxidation process was studied on three separate organosilicate films: a nominally dense film (no added porogen), a film containing 40% PS-P4VP, and a film with 40% L121 (designated MSSQ, PS-P4VP/Si, and L121/Si, respectively, as discussed in the Experimental Section). Briefly, the starting material used for these oxidation studies was a silsesquioxane that was spun-cast and upon curing formed a rigid organosilicate thin film. The nominally dense (no added porogen, only silsesquioxane) MSSQ film was actually a microporous material with an average pore size of <1 nm. The micropores in the organosilicate film were formed during curing of the silsesquioxane at 450 °C. PS-P4VP/Si and L121/Si films were spun as a mixture of the silsesquioxane and a block polymer. The block polymer contained a silsesquioxane compatible and incompatible domain that led to microphase separation. Treatment under nitrogen at 450 °C accomplished both curing of the silsesquioxane and thermal degradation of the polymer to yield mesoporous films with PS-P4VP/Si having the larger pore size. Pore size is largely determined by the concentration, block length, and interaction parameter.[25] Details of the pore size of each film will be discussed in detail with the ellipsometric porosimetry results.

Before oxidation, the silsesquioxane had been previously cured in nitrogen at 450 °C for 2 h and allowed to cool to room termperature, to set the resin and decompose any organic pore generators (porogen) in the film, creating a porous organosilicate. The organosilicate film was then exposed to an oxidizing environment in the presence of a combustible hydrocarbon fuel. Both the fuel and the oxidizer will physisorb to some extent on the surface of the organosilicate. This includes all pore surfaces that are accessible based on the interconnectivity of the material and the molecular size of the adsorbant. The physisorption process has been extensively studied and is similar to the process used in nitrogen and toluene porosimetry. Further, some fuel and oxidizer will be present in the vapor phase away from the porous surfaces and the interface. Because of the elevated temperature of the films during processing, the actual partial pressure in the chamber during oxidation was low relative to the values quoted at room temperature. Once the substrate reached the combustion temperature, the fuel began to combust on the surface at a rate that was dependent on temperature. Currently, the mechanism for the oxidation process is not certain; however, the following are two plausible proposals for the process. First, the combustion process releases energy that locally increases the temperature of the surface where the fuel is present. This local increase can be significant enough to increase the temperature above what is required for oxidation of the organosilicate initiating combustion. A second possibility is that the radical species generated in the combustion process attack and oxidize the organosilicate directly. Regardless of the mechanism, the oxidation process can be controlled by manipulating the spatial distribution of the fuel and oxidizer within the film.

We begin by examining the role of octane in different environments on organosilicate oxidation at a temperature of 450 °C. As described in the Experimental Section, the partial pressure of octane was controlled using two mass flow controllers, one of which was bubbled through octane using either nitrogen or oxygen as the carrier gas. Via examination of the contact angles, as shown in Table 1, it is clear that the presence of both octane and oxygen is required to reduce the contact angle. The films exposed to either nitrogen or oxygen alone both gave high values for the contact angle, clearly indicating the oxidizing agent alone is not responsible for the changes in surface energy. The addition of octane at $P_{2.5\%}|^{25C}$ or $P_{25\%}|^{25C}$ of the room-temperature saturation pressure to an oxygen-free nitrogen carrier gas stream also left the films unaltered; however, with oxygen and octane together, all three films became extremely hydrophilic with as little as $P_{0.025\%}|^{25C}$. Similarly, the thickness and refractive index of the films remained fairly constant when they were heated to 450 °C in the presence of pure nitrogen, pure oxygen, and mixtures of nitrogen and octane. However, mixtures of oxygen and octane led to a considerable decrease in the thickness and an increase in the refractive index as measured by ellipsometry. For each sample, the thickness and refractive index were fit to a one-layer model (Experimental Section for more details).

SIMS was chosen to examine the elemental depth profile because of the exquisite sensitivity of the technique relative to other depth profiling techniques, particularly for low elemental

Table 1. Contact Angles, Thicknesses, and Refractive Indices of the Dense and Porous Films Heated to 450 °C as a Function of the Environment[a]

	contact angle (deg)			thickness (nm)			refractive index at 650 nm		
type of carrier gas and partial pressure of octane	MSSQ	PS-P4VP/Si	L121/Si	MSSQ	PS-P4VP/Si	L121/Si	MSSQ	PS-P4VP/Si	L121/Si
control (N_2)	103	105	112	223	307	209	1.392	1.224	1.224
N_2 with $P_{2.5\%}\|^{25C}$	102	104	112	222	302	198	1.389	1.231	1.225
N_2 with $P_{25\%}\|^{25C}$	102	106	109	221	296	194	1.389	1.231	1.227
O_2 with $P_{0\%}\|^{25C}$	101	105	107	217	304	190	1.384	1.231	1.227
O_2 with $P_{0.025\%}\|^{25C}$	12	0	0	206	298	140	1.391	1.231	1.282
O_2 with $P_{0.25\%}\|^{25C}$	10	0	0	164	256	145	1.429	1.246	1.278
O_2 with $P_{2.5\%}\|^{25C}$	8	0	0	160	222	140	1.431	1.256	1.282

[a] $P_{x\%}|^{25C}$ indicates the saturation level of octane relative to room temperature. The control sample was subjected to no further treatment beyond the initial curing and porogen degradation step conducted in nitrogen, which was performed on all samples.

dx.doi.org/10.1021/am4023237 | ACS Appl. Mater. Interfaces 2013, 5, 9075−9087

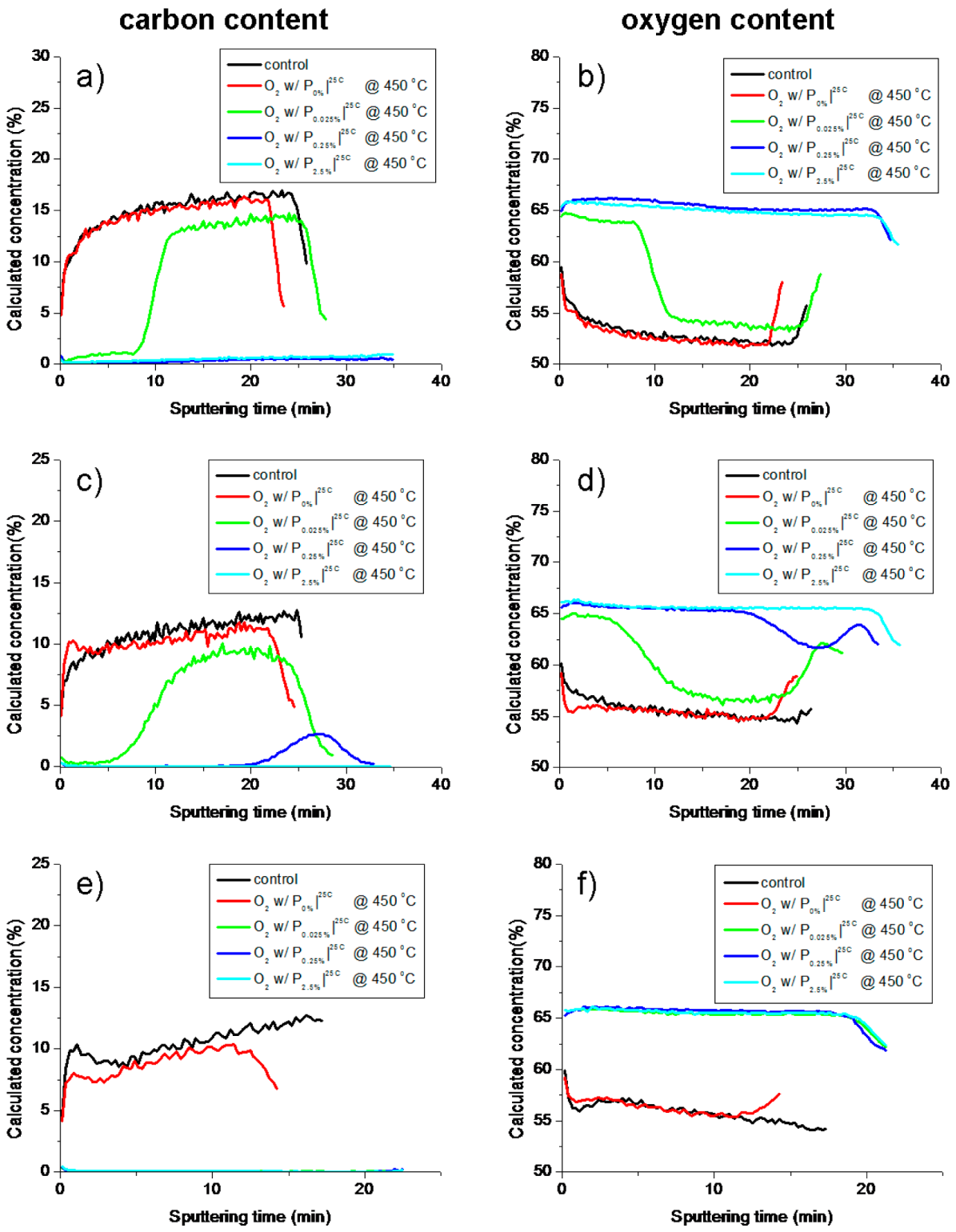

Figure 1. SIMS profile of (a) carbon and (b) oxygen for MSSQ, (c) carbon and (d) oxygen for PS-P4VP/Si, and (e) carbon and (f) oxygen for L121/Si. The figure legend displays the carrier gases and the percentages of octane relative to room-temperature saturation ($P_{x\%}|^{25C}$). The control sample was subjected to no further treatment beyond the initial curing and porogen degradation step conducted in nitrogen, which was performed on all samples.

concentrations. The elemental profiles as a function of depth are shown in Figure 1, to determine the uniformity of film oxidation. Panels a, c, and e of Figure 1 give the carbon content as a function of depth of MSSQ, PS-P4VP/Si, and L121/Si, respectively. Similarly, panels b, d, and f of Figure 1 display the oxygen content of MSSQ, PS-P4VP/Si, and L121/Si, respectively. The composition given by elemental percentage has been calculated from the secondary ion intensities using the method described in the Experimental Section. The quantification failed to accurately capture the composition of the underlying silicon layer as discussed. For this reason, the displayed data have been truncated at this interface; however, the unmodified secondary

dx.doi.org/10.1021/am4023237 | ACS Appl. Mater. Interfaces 2013, 5, 9075−9087

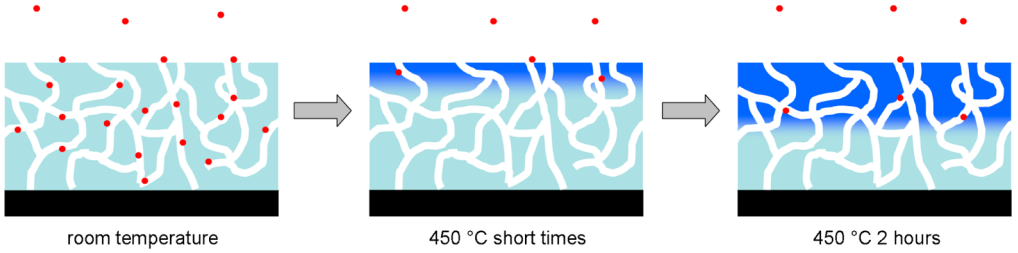

Figure 2. Schematic of the inhomogeneous oxidation process at 450 °C for a porous organosilicate film. Red dots represent molecular octane adsorbed to the surface or in the vapor phase. Light and dark blue represent unoxidized and oxidized organosilicate, respectively. Oxygen is abundant and present throughout but is not shown.

ion intensities are available in the Supporting Information. Each figure shows the depth profile for the control film that is cured and porogen decomposed in nitrogen as described in the Experimental Section, as well as the additional treatment in oxygen at 450 °C with varying levels of octane. In addition, we have examined treatments in nitrogen in the presence of octane for each film type (MSSQ, PS-P4VP/Si, and L121/Si). The films having this additional treatment in nitrogen with octane had depth profiles identical to that of the control film and are therefore not displayed in Figure 1. The unprocessed profiles for these films are available in the Supporting Information along with those of the other unprocessed films. It is reasonable to expect the composition of these films to remain unchanged as there was no change in the measured contact angle, thickness, and refractive index as shown in Table 1.

Figure 1 shows the oxygen-treated films (MSSQ, PS-P4VP/Si, and L121/Si) in the absence of octane had profiles identical to that of the nitrogen control for both carbon and oxygen, indicating the presence of oxygen at 450 °C does not lead to oxidation. On the contrary, the addition of octane to oxygen reduces the level of carbon and increases the level of oxygen within the film. Interestingly, this does not occur uniformly throughout the film but at the vapor–film interface and propagates through the film. This is apparent from the abrupt increase in the level of carbon and the decrease in the level of oxygen at intermediate sputtering times for the MSSQ and PS-P4VP-Si films treated at $P_{0.025\%}|^{25C}$ (Figure 1a–d). Higher octane concentrations led to films that were completely oxidized throughout the thickness. Further, PS-P4VP/Si porous samples (Figure 1c,d) showed transitions at both the $P_{0.025\%}|^{25C}$ and $P_{0.25\%}|^{25C}$ octane levels, indicating that the depth of the compositional transition in the film can be controlled by the concentration of octane in the vapor. Increasing the octane concentration beyond this point for either sample led to complete oxidation as occurred for the L121/Si porous films (Figure 1e,f) at all octane concentrations. In general, the reduction of carbon leads to a corresponding increase in the level of oxygen that explains the depth profile of the oxygen composition. Interestingly, there is also a noticeable peak in the oxygen concentration near the silicon interface for PS-P4VP/Si samples in oxygen at $P_{0.025\%}|^{25C}$ and $P_{0.25\%}|^{25C}$, which is attributed to a change in porosity. It is known that a porogen can accumulate at interfaces depending on the interactions with the underlying surface.[26,27] The increased porosity due to accumulation would lead to lower solid contents and more surface area near the interface causing the oxidation to proceed more rapidly. This explanation is consistent with the oxidation of L121/Si being more rapid that that of PS-P4VP/Si because of the smaller pore size.

This transition in the carbon and oxygen composition of the film can be rationalized by the spatial location of the octane combustion as described in Figure 2. At room temperature, fuel (red dots representing molecular octane) is adsorbed throughout the porous film. As the temperature is increased to 450 °C, the fuel combusts and becomes depleted throughout the film, leaving the film devoid of octane throughout its thickness. Oxygen is the carrier gas and is at a considerably higher concentration; therefore, it is assumed oxygen will not be the limiting reagent in the process. The initial temperature ramp will result in some oxidation from the fuel initially coated on the pores; however, this effect is minimal because of the small amount of octane present during the initial ramp. The oxidation primarily occurs once the temperature reaches 450 °C where the fuel combusts rapidly when it contacts the hot surface. Because combustion decreases the concentration of octane and this occurs rapidly as the octane approaches the hot interface, the distribution of octane will be inhomogeneous throughout the depth of the film, explaining the inhomogeneous oxidation for films that were not completely oxidized.

Combustion is a random process, and the octane will have a distribution of residence times prior to combustion. Initially, only the outer interface will be recognizably oxidized, but increasing the time will increase the probability of encountering longer-lived octane species that reach the inner portion. After 2 h, the oxidation front reached a certain point within the film and heat was removed, terminating the combustion. The octane concentration also plays a role in the depth of penetration of the oxide front. Low octane concentrations provide a lower probability of octane reaching the inner portion of the film; thus, only the vapor interface becomes oxidized, while the interior is largely unaffected. Increasing the octane concentration leads to a higher probability of octane reaching the inner portions of the film, which moves the oxidation front further toward the substrate. This process produces a material that resembles UV–ozone- and O_2 plasma-treated films where the reactive species are delivered from the vapor phase to the outer interface of the film creating compositionally inhomogeneous materials with a sharp oxidation front.

The films were also examined using Fourier transform infrared spectroscopy (FTIR), shown in Figure 3, to determine how the oxidation process affects chemical bonding within the film. Initially, the nitrogen-cured materials exhibit peaks consistent with the methyl silsesquioxane–silica copolymer. The silicon–carbon and silicon–oxygen modes are distinctive in the 1400–700 cm^{-1} range and can be used to provide information about bonding. Silicon–carbon modes are present at 775 cm^{-1}, representing the Si–C stretch, and 1275 cm^{-1}, representing the symmetric $Si(CH_3)_x$ deformation.[28] The Si–O–Si modes of the cured silsesquioxane appear at two locations: 1030 cm^{-1} indicative of a smaller-bond angle (<144°) networklike structure and 1140 cm^{-1} for the larger-bond angle (>150°) cagelike structures.[28] Silicon–carbon peaks of MSSQ remain unchanged

dx.doi.org/10.1021/am4023237 | ACS Appl. Mater. Interfaces 2013, 5, 9075–9087

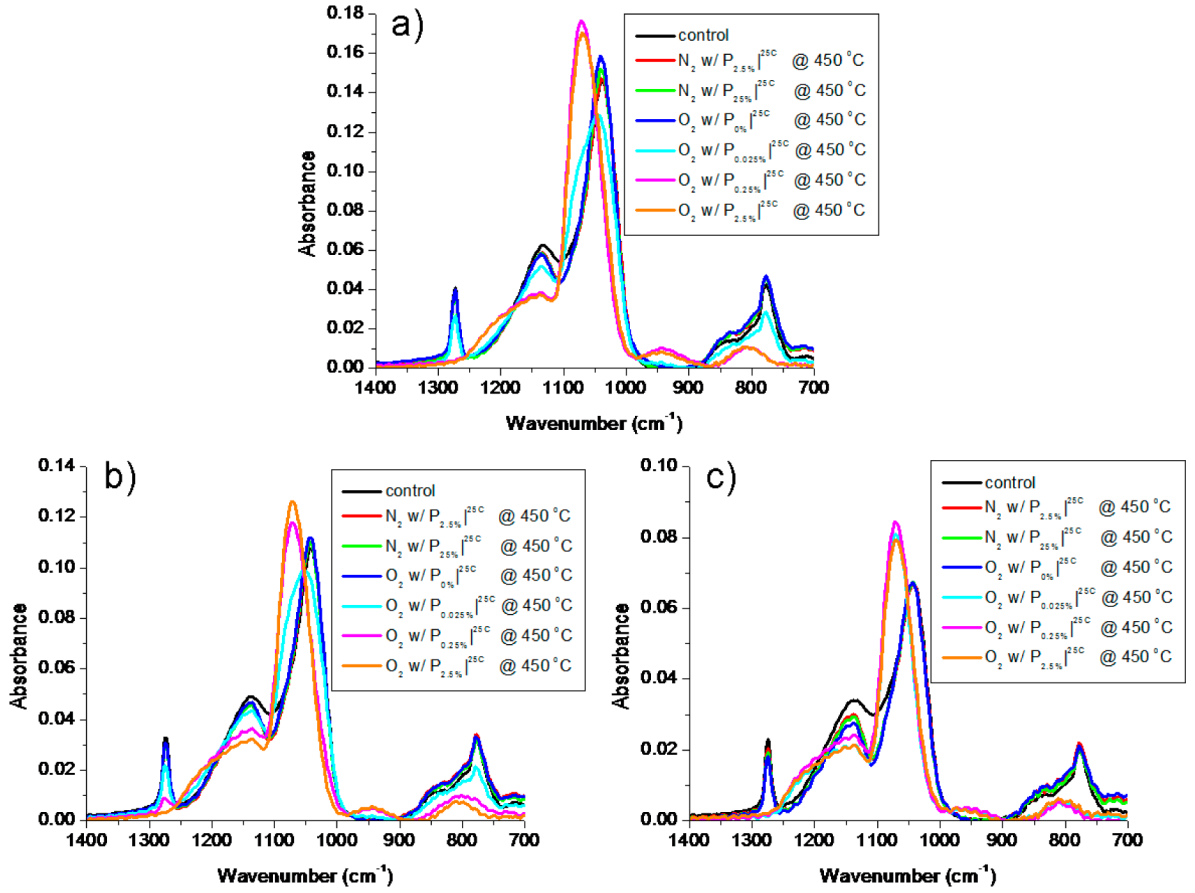

Figure 3. FTIR spectra of (a) MSSQ, (b) PS-P4VP/Si, and (c) L121/Si films after they had been heated at 450 °C in various environments. The figure legend displays the carrier gases and the percentages of octane relative to room-temperature saturation ($P_{x\%}|^{25C}$). The control sample was subjected to no further treatment beyond the initial curing and porogen degradation step conducted in nitrogen, which was performed on all samples.

upon heating at 450 °C in nitrogen for $P_{2.5\%}|^{25C}$ or $P_{25\%}|^{25C}$ octane as well as in oxygen without octane; however, the dip between the 1030 and 1140 cm^{-1} bands becomes slightly more pronounced, which is likely caused by silicon−oxygen reorganization due to further curing.[28] Heating in oxygen with octane causes a loss of the silicon−carbon peaks as expected from SIMS. Further, there is a decrease in the network- and cagelike Si−O−Si modes and the appearance of two new peaks at 935 and 1060 cm^{-1}.[28] The former is a Si−OH bending band signifying the presence of silanols, and the latter indicates a transformation to SiO_2 with a bond angle of ∼144°.[28] While intermediate stages of the oxidation appear at different octane concentrations for MSSQ and PS-P4VP/Si, L121/Si is completely transformed even at the lowest octane concentration as expected from the SIMS results. The oxidation of L121/Si is rapid relative to the oxidation of the other samples because of the large surface area and thin pore walls (high porosity but small pore size). The large surface area of the L121/Si samples causes an increased amount of fuel to be adsorbed and, therefore, a greater amount of combustion at a given temperature. Carbon−hydrogen and oxygen−hydrogen modes are also present in the 3800−2600 cm^{-1} range; however, they tend to be weak or broad relative to the silicon modes. For the sake of completeness, these have been provided in the Supporting Information.

From the thickness and refractive index measurements in Table 1, it is clear that all films were, at minimum, partially collapsing in the presence of octane and oxygen. We have examined the films using toluene adsorption ellipsometric porosimetry to determine the change in pore size after exposure to various environments at 450 °C. Ellipsometric porosimetry is a method of determining the pore size distribution (PSD) in a thin film by the adsorption and desorption of a condensable vapor (in this case toluene). When the Kelvin equation is applied, the adsorption isotherm yields information about the pore cavity size while the desorption isotherm provides information regarding the connection size for these cavities (i.e., the neck).[29] A schematic of the pore cavity and neck dimension has been provided previously.[30] The PSD plot of each sample discussed below will have at minimum of two peaks (and for these films only two), the larger being the cavity size distribution and the smaller being the neck size distribution between cavities.

The nominally dense and porous films exhibit dramatically different responses to the combustion treatment as shown in Figure 4. Panels a and b of Figure 4 show the toluene adsorption and desorption isotherms for MSSQ films treated under various conditions. Here the adsorption and desorption isotherms show minimal hysteresis, essentially overlaying one another for each sample. Panels c and e of Figure 4 show the pore size distributions calculated from the toluene adsorption isotherms for PS-P4VP/Si and L121/Si, respectively. Alternatively, panels d and f of Figure 4 give the pore size distributions from the desorption isotherms. The isotherms for the PS-P4VP/Si and L121/Si samples show a noticeable amount of hysteresis, leading to a difference in the calculated size for the cavity and neck as described above.

As expected, the nitrogen-cured MSSQ control film showed only microporosity, and the addition of octane to the nitrogen

dx.doi.org/10.1021/am4023237 | ACS Appl. Mater. Interfaces 2013, 5, 9075−9087

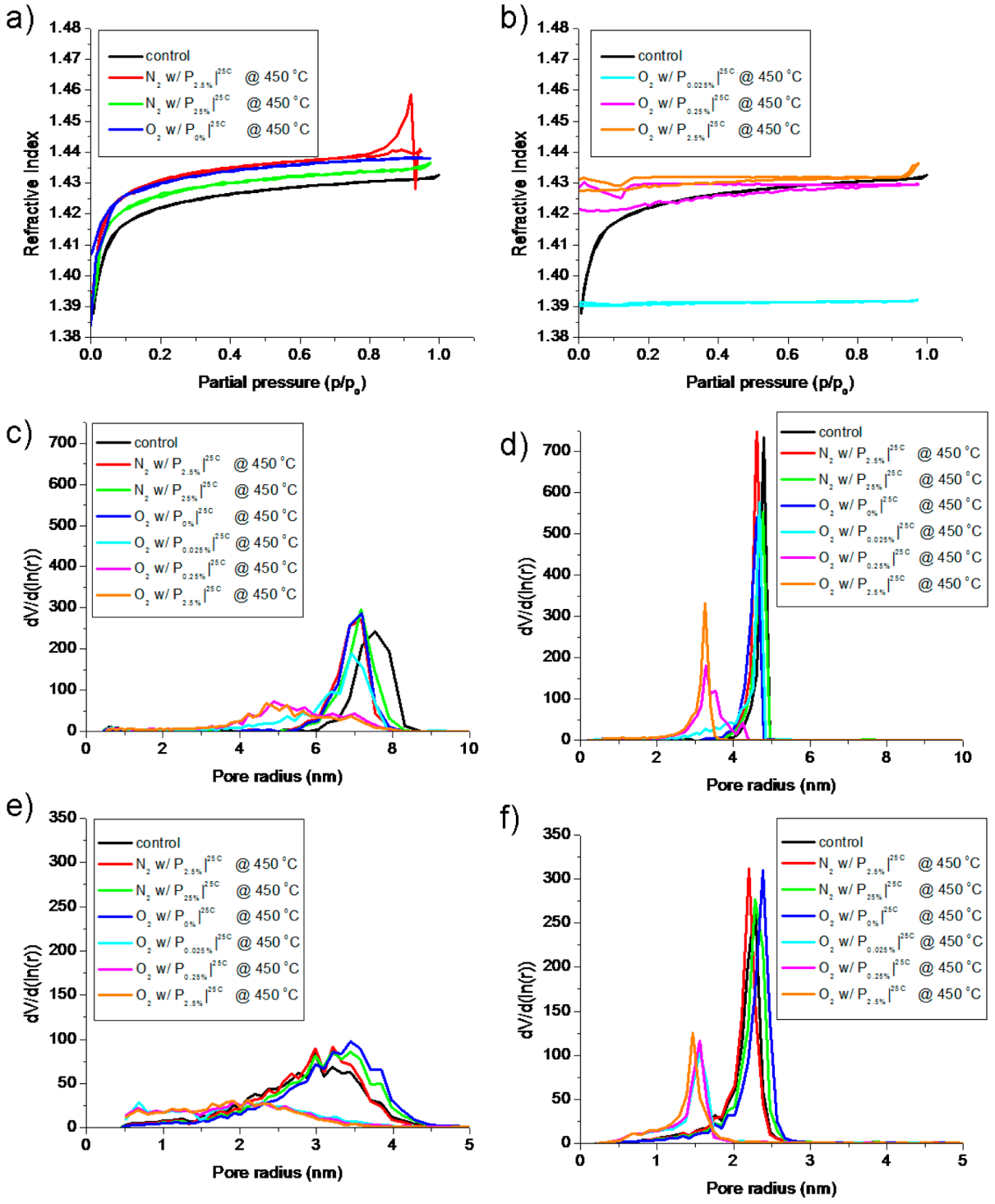

Figure 4. Toluene adsorption. Film refractive index vs toluene partial pressure for MSSQ samples treated (a) without and (b) with octane. Pore size distributions measured by toluene adsorption ellipsometric porosimetry and analyzed using the Kelvin equation from the (c) adsorption and (d) desorption isotherms for PS-P4VP/Si films and (e) adsorption and (f) desorption isotherms for L121/Si films. The figure legend displays the carrier gases and the percentages of octane relative to room-temperature saturation ($P_{x\%}|^{25C}$). The control sample was subjected to no further treatment beyond the initial curing and porogen degradation step conducted in nitrogen, which was performed on all samples.

atmosphere during curing had no effect on the toluene adsorption profile (Figure 4a). In fact, the isotherm profiles were identical to that of the film treated with oxygen without octane ($P_{0\%}|^{25C}$) also shown in Figure 4a. The sample treated in nitrogen with $P_{2.5\%}|^{25C}$ octane shows instability at high partial pressures, which is an artifact for partial condensation on the sample causing the refractive index and thickness to vary. However, all show nearly identical isotherm trends in the microporous range (low partial pressure). Interestingly and somewhat expectedly, microporous MSSQ films heated to 450 °C in the oxygen and octane environment subsequently did not adsorb toluene vapor. Figure 4b shows the refractive index versus toluene partial pressure for the $P_{0.025\%}|^{25C}$, $P_{0.25\%}|^{25C}$, and $P_{2.5\%}|^{25C}$ octane-treated samples along with the control sample. The constant refractive

dx.doi.org/10.1021/am4023237 | ACS Appl. Mater. Interfaces 2013, 5, 9075−9087

indices (lack of solvent adsorption) for samples treated with oxygen and octane indicate that the pore dimensions are now smaller than the dimension of the molecular adsorbent (in this case toluene). However, from SIMS and FTIR data, it is clear that while the bulk material has not been noticeably changed for the $P_{0.025\%}|^{25C}$ treatment, the $P_{2.5\%}|^{25C}$ sample has been completely oxidized. This is also obvious from their different refractive indices shown in Figure 4b (1.39 vs 1.43). Unlike panels c–f of Figure 4, which display the calculated pore size distributions from the refractive index profiles, panels a and b of Figure 4 were left as the raw refractive index profiles to show that the films treated in oxygen with octane at both $P_{0.025\%}|^{25C}$ and $P_{2.5\%}|^{25C}$ had no accessible porosity (constant refractive index profile) but different refractive indices relative to samples treated with nitrogen or oxygen but without octane. Because of the lack of toluene adsorption in these samples, no information about pore size could be obtained even though microporosity is likely present as indicated by the similarities in thickness and refractive index between the nitrogen control sample and oxygen-treated samples at $P_{0\%}|^{25C}$ and $P_{0.025\%}|^{25C}$ octane (Table 1). Further, the control, nitrogen samples, and oxygen-treated sample at $P_{0\%}|^{25C}$ octane (Figure 4a) clearly show toluene adsorption at partial pressures consistent with the microporous regime. Thus, use of the Kelvin equation requiring the formation of a meniscus is valid for only the mesoporous samples (PS-P4VP/Si and L121/Si) and cannot be applied to the microporous MSSQ films.[29]

Panels c–f of Figure 4 show the pore size distributions for the PS-P4VP/Si and L121/Si samples calculated from the toluene adsorption profiles using the Kelvin equation. Once again, there is no discernible change in the pore size distribution for the samples heated in nitrogen, nitrogen with octane, or pure oxygen for the PS-P4VP/Si or L121/Si films. However, for the samples processed in oxygen with octane, there is apparent collapse of the pores during oxidation. For the $P_{0.025\%}|^{25C}$ octane PS-P4VP/Si film shown in panels c and d of Figure 4, the presence of a tail on the small pore size is noticeable in both the adsorption and desorption curves, indicating a partial decrease in both cavity and neck size. With $P_{2.5\%}|^{25C}$ octane on oxygen on the PS-P4VP/Si sample, the pores have collapsed on average to ~65% of their original size and the cavity size distribution (Figure 4c) has broadened considerably. For the L121/Si films in panels e and f of Figure 4, the pores have also collapsed to approximately 65% of their original size even at the lowest level of octane in oxygen studied ($P_{0.025\%}|^{25C}$), and there is little change upon addition of more octane. This result is expected for this sample because both SIMS and FTIR data show complete oxidation for all octane concentrations in oxygen.

We also studied the fuel-oxidizer procedure for generating materials uniformly oxidized throughout the film thickness. Because oxidation occurs only in the presence of octane, controlling the location of the fuel should allow for control of the oxidation. Therefore, if the fuel is uniformly distributed throughout the film, combustion should proceed uniformly, leading to a homogeneous material. From the previous SIMS experiments, it is apparent that the octane fuel is depleted when it contacts the surface at elevated temperatures because the oxidation occurs at the vapor–film interface. In principle, if the temperature was reduced such that the rate of combustion was low relative to the rate of fuel exchange at the pore interface, it should be possible to generate a uniformly oxidized material. In practice, this was never observed because these experiments would require extremely long times at these slow rates of combustion. Alternatively, to generate uniformly oxidized materials, we chose a temperature cycling approach utilizing a temperature below the combustion temperature to replenish the adsorbed fuel layer on the organosilicate and a higher temperature where the combustion occurs. The rate of combustion is directly related to the temperature; therefore, with a fixed amount of fuel on the surface, higher temperatures will lead to a greater degree of combustion until the fuel is depleted. This protocol is designed to keep a relatively constant level of fuel on the surface by combusting only a small amount each cycle. In each experiment, 100% of the oxygen is bubbled through octane to obtain the highest level of fuel on the surface. As shown in Figure 5 at $P_{sat}|^{25C}$, the octane vapor (red dots) condenses within the pores (solid red within the pores), which, in practice, can be observed visually by a slight change in the color of the film. As the temperature is increased, the octane evaporates; however, a larger amount of octane remains on the material surface at $P_{sat}|^{25C}$ relative to the previous experiments performed at lower partial pressures. Once again, given that oxygen is the carrier gas and at a considerably higher concentration, the octane vapor is assumed to be abundant during the oxidation. The temperature cycles begin 50 °C below the maximal temperature, which is increased over a 10 min interval and subsequently decreased to 50 °C below the maximal temperature over a 15 min interval. As mentioned, this constitutes one cycle, and for each cycle, a certain percentage of the adsorbed fuel combusts. This percentage increases with temperature, as does, therefore, the degree of oxidation. With each cycle, the level of oxidation increases as represented in the schematic of Figure 5 at cycle 4 and the final cycle (cycle 8). In each case, the lowest temperature in the cycle is selected to be below the temperature at which any noticeable oxidation occurs, allowing the surface to re-equilibrate with fuel in the absence of significant combustion. Here the fuel is not combusting significantly at the outer interface but is able to recoat the inner portion of the pore surface. The maximal temperatures are chosen such that the lower maximal temperatures of the series provide a slow combustion and hence

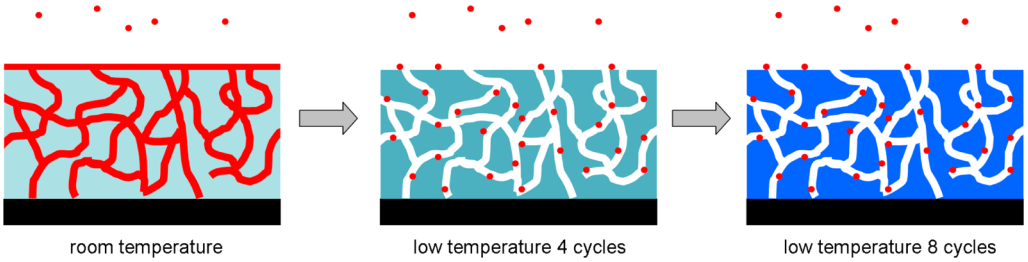

Figure 5. Schematic of the homogeneous oxidation process for a porous organosilicate film. Red dots represent molecular oxygen adsorbed to the surface or in the vapor phase, while solid red within the pores represents condensed liquid octane. The degree of oxidation is represented by the darkness of the blue color, with the lightest representing unoxidized organosilicate and the darkest representing oxidized organosilicate. Oxygen is abundant and present throughout but is not shown in the schematic.

Table 2. Contact Angles, Thicknesses, and Refractive Indices for the Dense and Porous Films Heated to Various Maximal Temperatures in Oxygen with $P_{sat}|^{25C}$ (except for the N_2 sample, which was the control that contained neither oxygen nor octane)

	contact angle (deg)			thickness (nm)			refractive index at 650 nm		
maximal temp	MSSQ	PS-P4VP/Si	L121/Si	MSSQ	PS-P4VP/Si	L121/Si	MSSQ	PS-P4VP/Si	L121/Si
N_2 (control)	103	105	112	223	307	209	1.392	1.225	1.224
280 °C	36	50	70	226	308	211	1.386	1.239	1.223
284 °C	10	30	40	225	303	200	1.389	1.233	1.234
285 °C	10	25	15	221	295	182	1.385	1.238	1.236
287 °C	15	20	10	221	294	162	1.387	1.249	1.293
295 °C	18	20	10	222	257	152	1.385	1.255	1.312

minimal oxidation, while the upper maximal temperatures fully oxidize the film. As stated above, the films are exposed to a total of eight cycles prior to the films being cooled to room temperature.

The contact angles, thicknesses, and refractive indices of films exposed to different maximal temperatures in the thermal cycling step are listed in Table 2. The contact angle of each film decreases considerably as would be expected for an oxidative process. There is a progressive decrease in thickness and an increase in refractive index with temperature for both the PS-P4VP/Si and L121/Si samples; however, the same change is not seen in the microporous MSSQ samples. It is expected that the oxidation will cause some shrinkage as was shown for the previous samples at 450 °C. The lack of shrinkage in the MSSQ could be from the micropores becoming inaccessible to octane because of pore sealing after the first round of combustion. As seen for the previous MSSQ samples heated to 450 °C in the presence of the fuel/oxygen mixture, toluene adsorption ellipsometric porosimetry showed that none of the temperature-cycled samples adsorbed toluene. Because toluene and octane have similar molecular dimensions, it seems that the lack of oxidation stems from the subsequent inaccessibility of the micropores to octane. This will be discussed further in the porosimetry section.

Figure 6 shows the carbon and oxygen depth profiles of the organosilicate films by SIMS analysis in a nitrogen control film together with films processed at different maximal temperatures in oxygen at room-temperature octane saturation. Given the lack of thickness change previously described, it is reasonable that there is little if any difference in the carbon and oxygen levels as a function of depth in the nominally dense MSSQ samples (Figure 6a,b). It is likely that some oxidation occurs at the outer interface because if the pores becomes sealed this would be the only surface exposed to the fuel. This would also be consistent with the decrease in contact angle reported in Table 2. The PS-P4VP/Si and L121/Si samples behave differently with a progressive increase in oxidation temperature. In each sample, the carbon content can be entirely removed and the oxygen concentration in the film increases at higher temperatures. Further, these transformations happen relatively uniformly throughout the film. Because of the larger pores of the PS-P4VP/Si sample, pore walls will be proportionately thicker at a given porosity and display a smaller surface area leading to slower oxidation. For example, while there is minimal bulk oxidation of the pores observed at 280 °C for PS-P4VP/Si, the L121/Si sample had a level of carbon noticeably lower than that of the L121/Si N_2 control sample. Further, L121/Si is completely oxidized by 287 °C, while PS-P4VP/Si requires temperatures up to 295 °C for complete oxidation under the process conditions studied.

We have also examined these films using FTIR as shown in Figure 7. As expected from the SIMS data, there is no apparent difference in the FTIR spectra for the MSSQ samples processed over the entire temperature range, consistent with a lack of substantial oxidation. However, PS-P4VP/Si and L121/Si films both show changes in the spectra that are characteristic of oxidation, such as loss of the peaks at 775 cm^{-1} representing the Si−C stretch and 1275 cm^{-1} representing the symmetric $Si(CH_3)_x$ deformation.[28] Once again, two new peaks appear at 935 and 1060 cm^{-1} characteristic of the silanol formation and transformation of the network- and cagelike Si−O−Si modes of SiO_2, respectively.[28]

The pore size distributions were also measured for samples processed at different cycle temperatures. The pore size distributions for PS-P4VP/Si and L121/Si are shown in Figure 8. The nominally dense MSSQ samples were omitted because all samples behaved identically from the perspective of porosity in a manner independent of the processing temperature. For each of the oxidized MSSQ samples, the refractive index of the films at 650 nm ranged only from 1.385 to 1.389, with no systematic variation in the data. Further, the samples were sealed to toluene in the vapor phase such that the film refractive index was independent of toluene partial pressure similar to the behavior seen in Figure 4a for the sample treated in oxygen with $P_{0.025\%}|^{25C}$ octane. Panels a and c of Figure 8 show the pore size distributions calculated from the toluene adsorption isotherms for PS-P4VP/Si and L121/Si, respectively. Alternatively, panels b and d of Figure 8 give the pore size distributions from the desorption isotherms. As described in Figure 4, the adsorption isotherm provides information about the cavity size while the desorption isotherm indicates pore neck size. PS-P4VP/Si samples shown in panels a and b of Figure 8 exhibited minimal changes in the pore size distribution at processing temperatures below 287 °C for either cavity or neck. This is true even when the film was >50% oxidized as estimated from SIMS data in Figure 6c. Thus, the films resist pore collapse even with substantial oxidation. Above this temperature (and therefore at higher levels of oxidation), both the cavities and necks show a considerable amount of pore collapse. L121/Si samples in panels c and d of Figure 8 show similar behavior, but the pore size reduction is complete by 287 °C. For both porogen types, the fully oxidized films for the low-temperature uniform oxidation treatment described here (maximal temperature of 295 °C) produced a pore size distribution similar to that produced by the fully oxidized high-temperature protocol with variable octane saturation (450 °C) described above.

The film modulus is an important parameter for controlling cracking and propagation. We also have examined the modulus of the films using ellipsometric porosimetry.[31] The modulus is determined by measuring the change in films thickness during the desorption stage of the ellipsometric porosimetry measurement; however, the analysis is restricted to a materials with a well-defined meniscus and therefore cannot be applied to the microporous MSSQ films. The measured modulii for PS-P4VP/Si and L121/Si films are listed in Table 3 for both the

dx.doi.org/10.1021/am4023237 | ACS Appl. Mater. Interfaces 2013, 5, 9075−9087

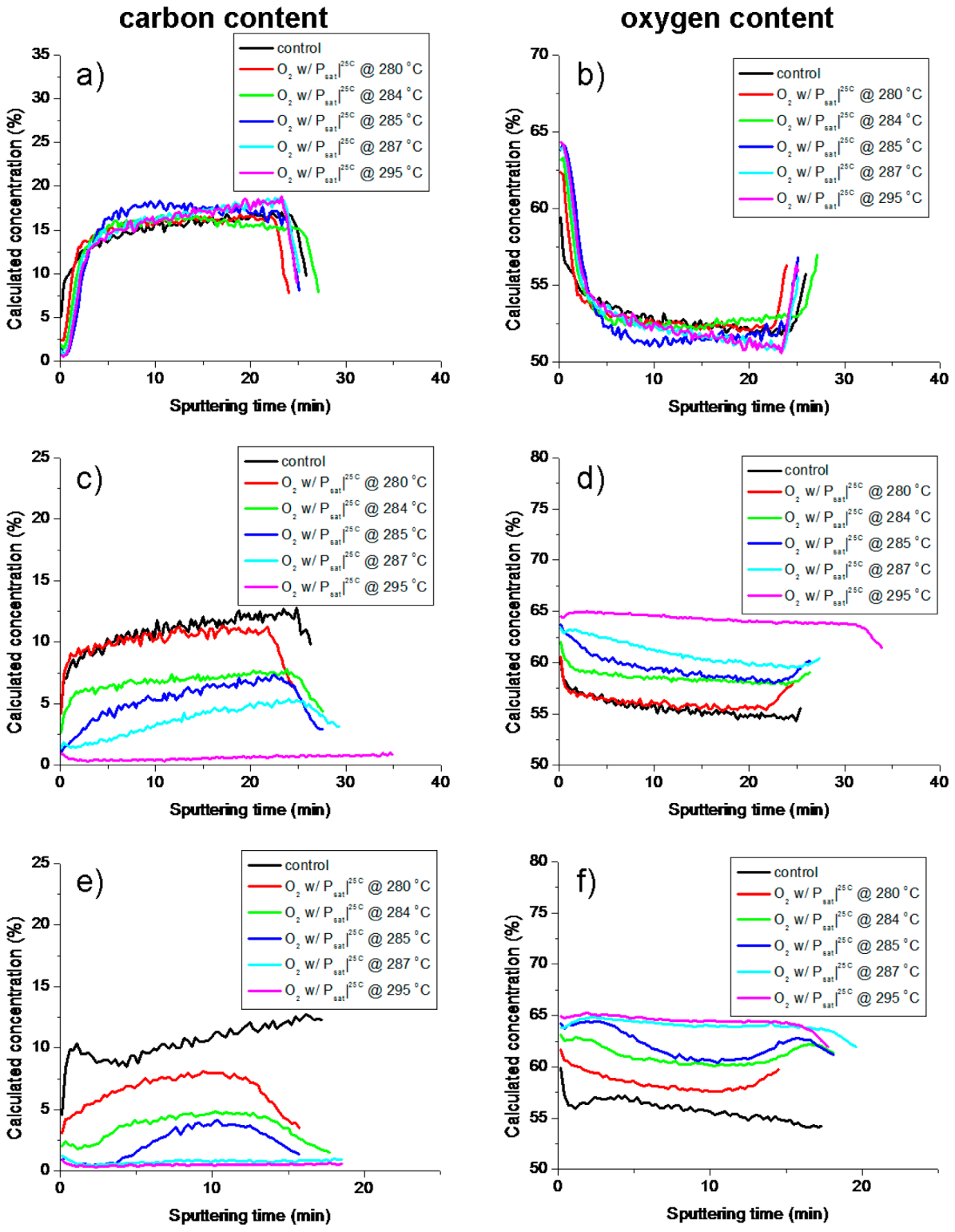

Figure 6. SIMS profiles of (a) carbon and (b) oxygen for MSSQ, (c) carbon and (d) oxygen for PS-P4VP/Si, and (e) carbon and (f) oxygen for L121/Si. The figure legend displays the carrier gases and maximal temperatures at room-temperature octane saturation. The control sample was subjected to no further treatment beyond the initial curing and porogen degradation step conducted in nitrogen, which was performed on all samples.

low-temperature uniform oxidation procedure and the high-temperature inhomogeneous oxidation.

Via examination of the series oxidized uniformly at lower temperatures (where the temperature was varied to control the level of oxidation), the trend indicates an increase in the modulus with the level of oxidation for both porogens. PS-P4VP/Si shows an approximately 70% increase in the modulus compared with that of the nitrogen-cured film and the fully oxidized film treated at 295 °C, while the L121/Si films show a 150% increase. From SIMS (Figure 6) and FTIR (Figure 7) analyses, it is clear that the oxidation level is increased for L121/Si relative to that of PS-P4VP/Si at any given temperature, which is also

dx.doi.org/10.1021/am4023237 | ACS Appl. Mater. Interfaces 2013, 5, 9075−9087

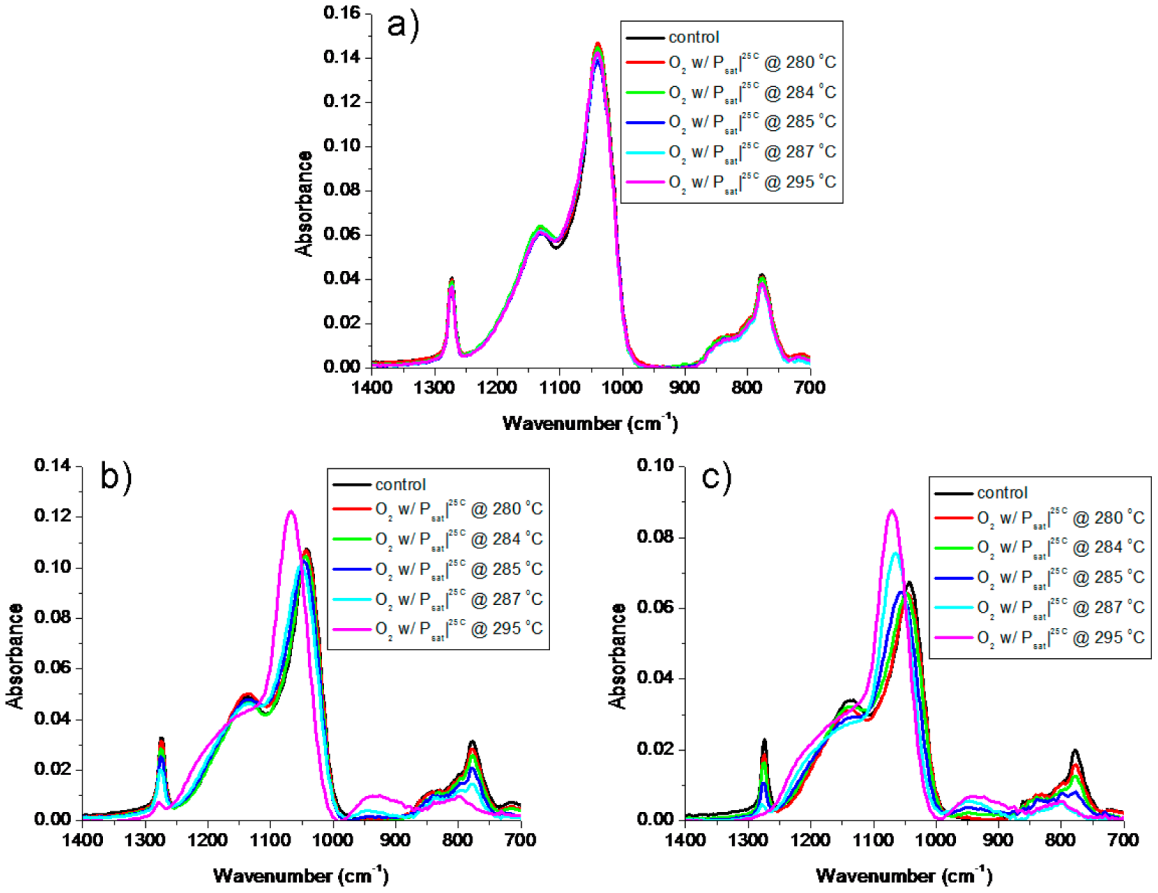

Figure 7. FTIR spectra of (a) MSSQ, (b) PS-P4VP/Si, and (c) L121/Si films. The figure legend displays the maximal temperatures in oxygen at room-temperature octane saturation. The control sample was subjected to no further treatment beyond the initial curing and porogen degradation step conducted in nitrogen, which was performed on all samples.

Table 3. Young's Moduli for Organosilicate Samples Heated in Various Environments[a]

	modulus (GPa) for uniform oxidation			modulus (GPa) for inhomogeneous oxidation	
maximal temperature of the eight-cycle process in O_2 at $P_{sat\%}\|^{25C}$	PS-P4VP/Si	L121/Si	environment at 450 °C for 2 h	PS-P4VP/Si	L121/Si
N_2 (control)	0.86	0.77	N_2 with $P_{2.5\%}\|^{25C}$	1.02	0.95
280 °C	0.77	0.84	N_2 with $P_{25\%}\|^{25C}$	1.12	1.02
284 °C	0.81	0.93	O_2 with $P_{0\%}\|^{25C}$	1.04	1.07
285 °C	0.88	1.25	O_2 with $P_{0.025\%}\|^{25C}$	1.29	1.76
287 °C	0.97	1.99	O_2 with $P_{0.25\%}\|^{25C}$	1.53	1.88
295 °C	1.46	1.82	O_2 with $P_{2.5\%}\|^{25C}$	2.08	1.73

[a]The N_2 sample is a control with no additional treatment, and $P_{x\%}|^{25C}$ indicates the saturation level of octane relative to that at room temperature.

consistent with the greater increase in the modulus for the L121/Si films.

For the inhomogeneously oxidized series at 450 °C using different levels of octane fuel, the trend also shows an increase in the modulus with oxidation level. Interestingly, there is a slight increase in the modulus of ∼15−20% with further curing at 450 °C, as demonstrated by comparing the initial nitrogen-cured control for both PS-P4VP/Si and L121/Si (displayed in the first series) with the respective octane and nitrogen and pure oxygen processed samples. The latter samples (O_2, N_2 at $P_{2.5\%}|^{25C}$, and N_2 at $P_{25\%}|^{25C}$) had nearly identical moduli for each series (PS-P4VP/Si or L121/Si), indicating that neither octane in nitrogen nor oxygen alone was a factor. Therefore, this is likely due to the increased heating time at 450 °C that causes additional cross-linking and restructuring within the film. The increase in the modulus from oxidation at $P_{2.5\%}|^{25C}$ octane in oxygen for the PS-P4VP/Si and L121/Si samples is approximately 100% for each film relative to that of samples cured in oxygen alone. It also appears that oxidation at the lower temperatures of 287 and 295 °C is enough to fully cure the material as the measured modulus of those L121/Si samples is similar to the modulus of those cured in oxygen with octane at 450 °C.

Finally, functionalization of organosilicate materials is often critical to their application. Silane coupling chemistry is used to generate specific chemical functionality depending on the application. The coupling occurs though available silanols on the surface. Because we previously mentioned that FTIR results indicate the appearance of silanols upon oxidation, we have studied the reactivity of these silanols with a standard silylating agent, *N*,*O*-bis(trimethylsilyl)acetamide. Silylation studies were performed on

dx.doi.org/10.1021/am4023237 | ACS Appl. Mater. Interfaces 2013, 5, 9075−9087

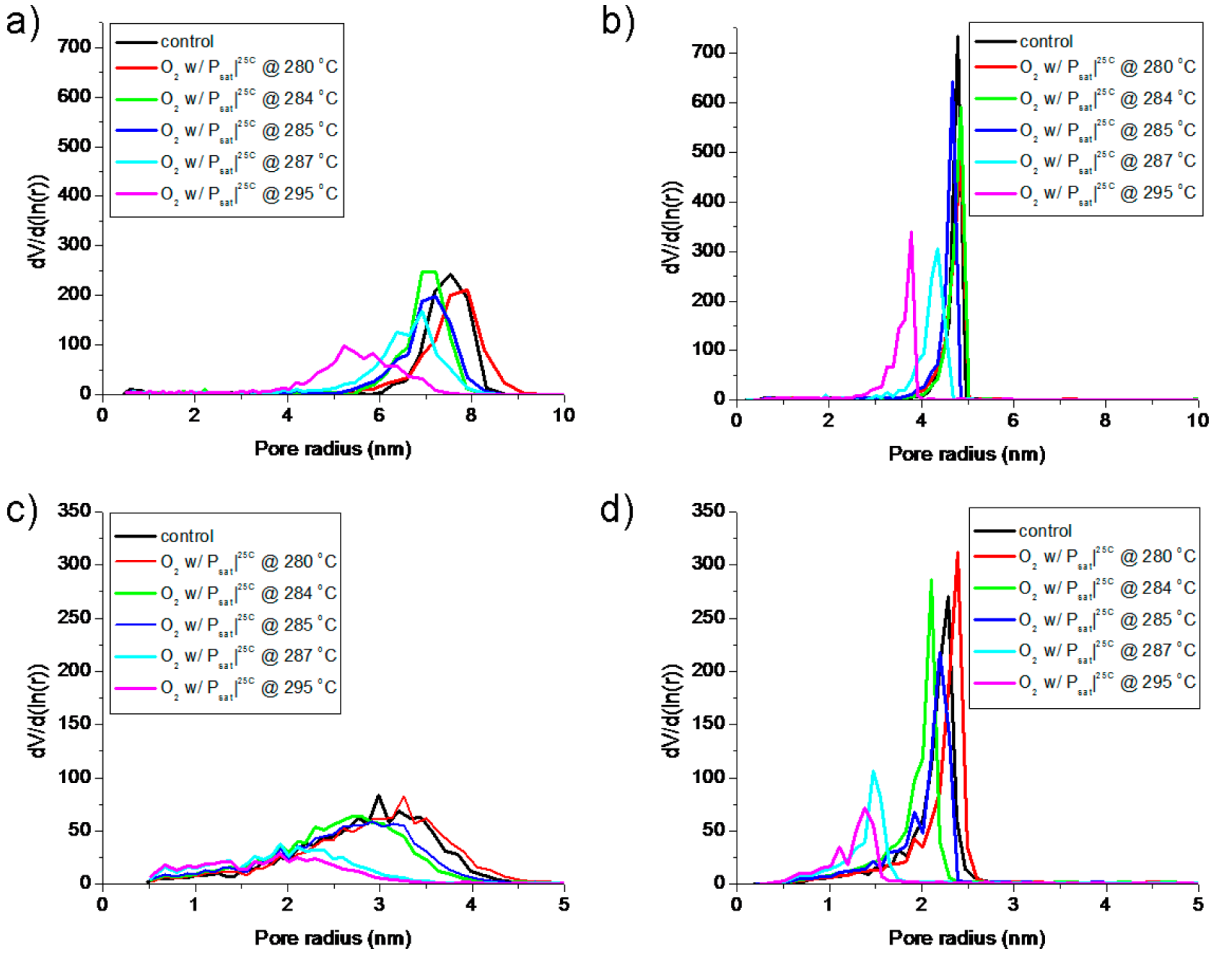

Figure 8. Pore size distributions measured by toluene adsorption ellipsometric porosimetry and analyzed using the Kelvin equation from the (a) adsorption and (b) desorption isotherms for PS-P4VP/Si and (c) adsorption and (d) desorption isotherms for L121/Si films. The figure legend displays the maximal temperatures in oxygen at room-temperature octane saturation. The control sample was subjected to no further treatment beyond the initial curing and porogen degradation step conducted in nitrogen, which was performed on all samples.

samples treated at 450 °C in oxygen at $P_{2.5\%}|^{25C}$. Prior to silylation, the contact angles for the oxidized MSSQ, PS-P4VP/Si, and L121/Si films were 8°, 0°, and 0°, respectively, as listed in Table 1. After treatment for 1 h with *N*,*O*-bis(trimethylsilyl)acetamide, the contact angles increased to 102°, 106°, and 112°, respectively. These values are essentially identical to the initial values of the nitrogen-cured material signifying a high level of accessible surface functionalization.

CONCLUSION

We have described a protocol for low-temperature oxidation of cured methylsilsesquioxane samples using a fuel and an oxidizer. Because the oxidation is confined to the location of the fuel, it is possible to impart a level of control not typically observed for current oxidative processes. Two-layer structures with an oxidized outer layer and uniformly oxidized films with a controlled level of oxidation have been produced. Given the intrinsic level of control, it is likely that gradient films could be produced using intermediate temperatures at which oxidation would proceed more rapidly at the vapor interface while still allowing some fuel to reach the substrate interface. Oxidation is accompanied by the transformation of cage- and networklike silsesquioxanes to tetrahedral SiO_2. Depending on the processing conditions, films can be oxidized uniformly or produce two-layer films with a sharp oxide−organosilicate interface. Although the process can cause some film shrinkage with collapse of porosity at high levels of conversion to oxide, if interrupted prior to complete conversion, the pore size is largely maintained. This simple oxidation process can also uniquely seal the film microporosity at the exposed surface, preventing adsorption of hydrocarbon vapors. Oxidation is accompanied by an increase in the Young's modulus, which should cause the films to be more resistant to cracking. Finally, the surfaces can be readily functionalized using standard silane chemistry, making this process valuable in numerous applications.

ASSOCIATED CONTENT

Supporting Information

Raw SIMS data. This material is available free of charge via the Internet at http://pubs.acs.org.

AUTHOR INFORMATION

Corresponding Author

*E-mail: rdmiller@us.ibm.com.

Funding

Notes

The authors declare no competing financial interest.

■ ACKNOWLEDGMENTS

We thank Andrew Kellock for his contributions to the SIMS quantification. We also thank JSR Corp. for providing the silsesquioxane materials used in this study. This work has been partially funded by National Science Foundation GOALI Grant ECCS-0823827.

■ ABBREVIATIONS

MSSQ, methylsilsesquioxane
PS-P4VP/Si, films cast using 40 wt % poly(styrene-*b*-4-vinyl pyridine)
L121/Si, films cast using 40 wt % Pluronic L121

■ REFERENCES

(1) Brown, W. D. In *Dielectric Material Integration for Microelectronics*; The Electrochemical Society: Pennington, NJ, 1998.
(2) Barwicz, T.; Popović, M. A.; Gan, F.; Dahlem, M. S.; Holzwarth, C. W.; Rakich, P. T.; Ippen, E. P.; Kärtner, F. X.; Smith, H. I. Reconfigurable silicon photonic circuits for telecommunication applications. In *Lasers and Applications in Science and Engineering*; International Society for Optics and Photonics: Bellingham, WA, 2008; pp 68720Z−68720Z-12.
(3) Holzwarth, C.; Barwicz, T.; Smith, H. I. *J. Vac. Sci. Technol., B: Nanotechnol. Microelectron.: Mater., Process., Meas., Phenom.* **2007**, *25* (6), 2658−2661.
(4) Kannan, R. Y.; Salacinski, H. J.; Butler, P. E.; Seifalian, A. M. *Acc. Chem. Res.* **2005**, *38* (11), 879−884.
(5) Hartmann-Thompson, C. In *Applications of polyhedral oligomeric silsesquioxanes*; Springer-Verlag: Dusseldorf, Germany, 2011.
(6) Chua, C.; Sarkar, G.; Chooi, S.; Chan, L. *J. Mater. Sci. Lett.* **1999**, *18* (17), 1437−1439.
(7) Maddalon, C.; Barla, K.; Denis, E.; Lous, E.; Perrin, E.; Lis, S.; Lair, C.; Dehan, E. *Microelectron. Eng.* **2000**, *50* (1), 33−40.
(8) Padovani, A. M.; Rhodes, L.; Riester, L.; Lohman, G.; Tsuie, B.; Conner, J.; Allen, S. A. B.; Kohl, P. A. *Electrochem. Solid-State Lett.* **2001**, *4* (11), F25−F28.
(9) Volksen, W.; Miller, R. D.; Dubois, G. *Chem. Rev.* **2010**, *110* (1), 56−110.
(10) Schmid, G. M.; Carpenter, L. E.; Liddle, J. A. *J. Vac. Sci. Technol., B: Nanotechnol. Microelectron.: Mater., Process., Meas., Phenom.* **2004**, *22* (6), 3497−3502.
(11) Hu, Y.; Bouamrani, A.; Tasciotti, E.; Li, L.; Liu, X.; Ferrari, M. *ACS Nano* **2010**, *4* (1), 439−451.
(12) Min, Q.; Wu, R.-a.; Zhao, L.; Qin, H.; Ye, M.; Zhu, J.-J.; Zou, H. *Chem. Commun.* **2010**, *46* (33), 6144−6146.
(13) Fan, J.; Gallagher, J. W.; Wu, H.-J.; Landry, M. G.; Sakamoto, J.; Ferrari, M.; Hu, Y. *J. Visualized Exp.* **2012**, *62*, e3876.
(14) Bass, J. D.; Grosso, D.; Boissiere, C.; Belamie, E.; Coradin, T.; Sanchez, C. *Chem. Mater.* **2007**, *19* (17), 4349−4356.
(15) Dunphy, D. R.; Singer, S.; Cook, A. W.; Smarsly, B.; Doshi, D. A.; Brinker, C. J. *Langmuir* **2003**, *19* (24), 10403−10408.
(16) Arkles, B.; Steinmetz, J.; Zazyczny, J.; Mehta, P. *J. Adhes. Sci. Technol.* **1992**, *6* (1), 193−206.
(17) Turri, S.; Levi, M. *Macromol. Rapid Commun.* **2005**, *26* (15), 1233−1236.
(18) Kim, H.-C.; Kreller, C. R.; Tran, K. A.; Sisodiya, V.; Angelos, S.; Wallraff, G.; Swanson, S.; Miller, R. D. *Chem. Mater.* **2004**, *16* (22), 4267−4272.
(19) Singh, S. K.; Kumbhar, A. A.; Dusane, R. *Mater. Lett.* **2006**, *60* (13), 1579−1581.
(20) Goldman, M.; Graves, D.; Antonelli, G.; Behera, S.; Kelber, J. *J. Appl. Phys.* **2009**, *106* (1), 013311−013311-7.
(21) Iijima, T.; Lin, Q.; Chen, S.; Labelle, C.; Fuller, N.; Ponoth, S.; Cohen, S.; Lloyd, J.; Dunn, D.; Muzzy, C. In *BEOL integration of highly damage-resistant porous ultra low-K material using direct CMP and via-first process*; Interconnect Technology Conference, 2006 International; IEEE: New York, 2006; pp 21−23.
(22) Sun, J.-N.; Gidley, D. W.; Hu, Y.; Frieze, W. E.; Ryan, E. T. *Appl. Phys. Lett.* **2002**, *81* (8), 1447−1449.
(23) Shamiryan, D.; Baklanov, M.; Vanhaelemeersch, S.; Maex, K. *J. Vac. Sci. Technol., B: Nanotechnol. Microelectron.: Mater., Process., Meas., Phenom.* **2002**, *20* (5), 1923−1928.
(24) Baklanov, M.; Mogilnikov, K.; Polovinkin, V.; Dultsev, F. *J. Vac. Sci. Technol., B: Nanotechnol. Microelectron.: Mater., Process., Meas., Phenom.* **2000**, *18* (3), 1385−1391.
(25) Leibler, L. *Macromolecules* **1980**, *13* (6), 1602−1617.
(26) Baklanov, M.; Maex, K.; Green, M. In *Dielectric films for advanced microelectronics*; Wiley: New York, 2007; Vol. *12*.
(27) Maidenberg, D. A.; Volksen, W.; Miller, R. D.; Dauskardt, R. H. *Nat. Mater.* **2004**, 3 (7), 464−469.
(28) Klymko, N. *Future Fab International* 2004, (17).
(29) Haynes, J. *Mater. Constr. (Paris)* **1973**, *6* (3), 209−213.
(30) Feller, B. E.; Lee, V. Y.; Virwani, K.; Knoesen, A.; Miller, R. D. *Chem. Mater.* **2013**, *25*, 2441−2449.
(31) Mogilnikov, K.; Baklanov, M. *Electrochem. Solid-State Lett.* **2002**, *5* (12), F29−F31.